# Electrodiffusion model of synaptic potentials in dendritic spines

Thibault Lagache[1,3,4], Krishna Jayant[1,2,3,4] and Rafael Yuste[1,3,4]

[1]Department of Biological Sciences, Columbia University, New York10027
[2]Department of Electrical Engineering, Columbia University, New York10027
[3]Neurotechnology Center, Columbia University, New York10027
[4]Kavli institute of Brain Science, Columbia University, New York, 10027

**ABSTRACT**

When modeling current flow in neurons, traditional cable theory ignores electrodiffusion (i.e. the interaction between the electric field and ionic diffusion) as it assumes that concentration changes associated with ionic currents are negligible. This assumption, while true for large neuronal compartments, fails when applied to femto-liter size compartments such as dendritic spines - small protrusions that form the main site of glutamatergic input in the brain. Here, we use the Poisson (P) and Nernst-Planck (NP) equations which relate electric field to charge and couple Fick's law of diffusion to electric field, to model ion concentration dynamics in dendritic spines. We use experimentally measured voltage transients from spines with nanoelectrodes to explore these effects with realistic parameters. We find that (i) passive diffusion and electrodiffusion jointly affect the kinetics of spine excitatory post-synaptic potentials (EPSPs); (ii) spine geometry plays a key role in shaping EPSPs; and, (iii) the spine-neck resistance dynamically decreases during EPSPs leading to short term synaptic facilitation. Our formulation can be easily adopted to model ionic biophysics in a variety of nanoscale bio-compartments.

## INTRODUCTION

Dendritic spines, nanoscale bulbous protrusions located along dendrites of principal neurons, form the primary site of excitatory synaptic input in the mammalian brain (1, 2). Their function and plasticity are essential for neuronal function, memory formation and brain development (3, 4). Excitatory neurotransmitters released during synaptic transmission activate receptors on the spine head, which causes ion channels to open and current to flow into the spine. This current charges the spine causing an excitatory post-synaptic potential (EPSP), which subsequently integrates onto the dendrite and summates with other synaptic inputs on its way to the soma and axon initial segment (5). When this summation crosses a particular threshold, the neuron fires an action potential (AP). Spines thus present the first node in the path of neuronal integration, and the voltage dynamics (i.e. rise time, fall time and amplitude) within a spine during synaptic input determine the characteristics of the downstream signal. Voltage recordings from this nanoscale neuronal subdomain have been challenging, and measurements have traditionally been at odds with each other, specifically with regard to the spine head EPSP magnitude (6-11) and neck resistance values (6, 7, 11-15). Recently however, optical and electrical recordings have reported fast and large EPSP values in the spine with high neck resistances (7, 9, 14, 16). But, given that spines exhibit a stereotypical, but highly variable geometry (17) comprising a bulbous head (volume ~ 0.01-0.3 $\mu m^3$) connected to the parent dendrite across a narrow neck (length ~ 1 μm; diameter ~ 50-150 nm), there is a need for models that elucidates the relationship between geometry and voltage dynamics during synaptic inputs. Such models will help reconcile the different values that have been experimentally procured and possibly help shed intuition on the reasons for the discrepancies in literature.

Traditionally, spine biophysics and the EPSP map across a neuron is modeled using cable theory (CT) (18-22). The cable equations treat the membrane as an RC circuit and compute the time evolution of the signal usually in the form of partial differential equations. This formulation neglects the effect of concentration gradients, which is a reasonable hypothesis for large neuronal compartments (such as the original squid giant axon) but may fail to accurately describe electrostatics in nanoscale structures such as dendritic spines. In addition, neck resistance has been indirectly estimated with fluorescence recovery after photo-bleaching (FRAP) time constants (12, 13, 23, 24) (i.e. charged or uncharged dye molecules diffusing back into the spine head upon a spine head photo-bleaching). Here, the mean escape time $\tau_e$ of a single diffusive molecule (with diffusion coefficient D) from the spine head into

the dendrite can be described by the relation(25) $\tau_e = D^{-1}\left(\frac{V}{4r} + \frac{L^2}{2} + \frac{VL}{\pi r^2}\right) + O(1)$, where V is the volume of the spine head, r the radius of the cylindrical neck and L its length. For a typical spine with head volume V = 0.1 μm$^3$, neck length L = 1 μm, neck radius r = 50 nm and a diffusion constant D = 0.5 x 10$^3$ μm$^2$ s$^{-1}$ (corresponding to the measured coefficient of calcium or sodium ions in cytoplasm) (26, 27), we obtain that $\frac{V}{4Dr} \approx \frac{L^2}{2D} = 1\,ms$ and $\frac{VL}{D\pi r^2} = 25\,ms$. Thus, in most spine geometries we can approximate $\tau_e \approx \frac{VL}{D\pi r^2}$, which is then used to fit the exponential decay rate of the FRAP transient. Neck resistance is finally estimated with $R_{neck} = R_{cyt}\frac{L}{\pi r^2} = R_{cyt}\frac{D\tau_e}{V}$, where $R_{cyt}$, the longitudinal cytoplasmic resistivity, is assumed to be constant $\approx 1 - 1.5\ \Omega.\mathrm{m}$ (10, 21)

While both cable theory and FRAP measurements have largely been used to model and extract spine biophysical parameters (6, 13, 20, 24), they do have limitations and many of the values are at odds with many experiments (8, 10, 23). As previously mentioned, one critical aspect that is ignored in cable theory is electrodiffusion (28-31) (i.e. the effect of the electric field on the concentration gradient), which is important when large longitudinal voltage gradients and concentration changes occur. This aspect becomes more critical in the small dendritic spines where sizeable voltage swings, large concentration changes on the order ~mM, and appreciable electric field gradients across a nanoscale neck can occur within a few milliseconds. Such effects could modulate both voltage and current transmission at a fundamental level.

In order to accurately describe electrolyte dynamics in biological micro-domains and explicitly account for the effect of geometry and electrodiffusion, the Poisson-Nernst-Planck (PNP) formalism is ideal (32) . However, the PNP equations cannot be solved analytically in complex three-dimensional structures, specifically in structures such as dendritic spines. Previous works that have focused on modelling electrodiffusion effect in spines (28, 33) have either captured the effects of the PNP purely through numerical simulations (11), examined dynamics under non-electroneutral conditions (34), or failed to corroborate the findings against experimental data with relevant time scales (28). Here, we use singular perturbation theory and derive coarse-grained PNP equations to describe voltage dynamics in the spine head during synaptic input, explicitly accounting for the effect of geometry and electrodiffusion. We find that electrodiffusion can play a significant role in determining the overall EPSP magnitude and time scales. Moreover, and in contrast to cable theory analysis, we show that electrodiffusion predicts current modulation across the neck on a millisecond

time scale, which suggests that the neck resistance can dynamically vary as a function of synaptic current. We use recently published measurements of spontaneous EPSP transients from spines to highlight these effects under different geometries.

## RESULTS

### PNP formalism

We used singular perturbation theory and analyzed the dynamics of both positive and negative charges inside the spine head and neck (Fig. 1a), and derived a novel coarse-grained system of equations that fully captures the coupled dynamics of ions and voltage with the PNP formalism. It uses a coupled system of two differential equations to describe the interacting ion and electrical potential dynamics: (1) the Poisson (P) equation (Eq. 1) that computes the electrical potential rising from the local differences between the concentrations of negative $c^-(x, t)$ and positive $c^+(x; t)$ charges,

$$\Delta_x \Phi(x,t) = \frac{e}{\epsilon_c}\left(c^-(x,t) - c^+(x,t)\right) \quad (1)$$

Where, $\Delta_x = \nabla_x^2$ is the Laplacian operator, $e$ the elementary electrical charge and $\varepsilon_c$ the electrical permittivity of the cytoplasm, and (2), the Nernst-Planck (NP) equation (Eq. 2) which captures the contribution of the electrical field on the concentration gradient;

$$\frac{\partial c}{\partial t}(x,t) = D\nabla.[\nabla.c + v\gamma c\nabla.\Phi](x,t) \quad (2)$$

Where, $D$ is the diffusion constant (that we assumed to be the same for both positive and negative charges), $\gamma = \frac{e}{kT}$ , and$v = \pm 1$, is the ionic valence. An analytical solution to the full system of PNP equations is not possible and hence must be either numerically computed or asymptotically estimated.

### Modeling electrostatics in the spine head and neck

We approximated the geometry of the dendritic spine with a ball (spine head, radius R) connected to the parent dendrite across a cylindrical thin neck (length L, varying cross-section $S(l) = \pi a(l)^2, 0 \leq l \leq L$) (Fig. 1a). We assumed that the neck radius is much smaller than the head radius $a(l) \ll R$, as corroborated by ultra-structural reconstructions (17) (Fig. 1b) and super-resolution microscopy of living spines(13). We modeled the spine head membrane as an impermeable membrane (no ion leak), with thickness d and small electrical permittivity $\epsilon_m \ll \epsilon_c$ (Fig. 1a, inset) (Table 1). We also assumed the continuity of the electrical field (derivative of the electrical potential) at the membrane boundary, a boundary

layer condition employed to solve electrostatic equations across dielectric layers (35, 36). Finally, boundary conditions for the potential and ion concentrations at the neck entrance were matched to physiological solutions inside the spine neck.

To mathematically analyze the PNP equations within the spine head, we applied the singular perturbation method using dimensionless variables, and approximate solutions (i.e. asymptotic expansions). Specifically, the dimensionless system of variables is given by $u = \frac{r}{R}, \phi(u,t) = \gamma\Phi(r,t),\ p(u,t) = \frac{c^+(r,t)}{c_0}$ and $(u,t) = \frac{c^-(r,t)}{c_0}$ , with $0 \leq r \leq R$ the radial coordinate within the spine head and $c_0$ the total concentration of positive (negative) ions inside the spine cytoplasm at resting state (Table 1). The reduced Poisson equation (Eq. 3) then read (see SI-I-A for details),

$$\delta_1 \Delta_u \phi(u,t) = n(u,t) - p(u,t) \quad (3)$$

where $\Delta_u$ is the Laplace operator in dimensionless variable u. Here $\delta_1 = \frac{\epsilon_c}{e\gamma c_0 R^2} = 2\left(\frac{\lambda_D}{R}\right)^2 \ll 1$, with $\lambda_D$ the Debye length ($\lambda_D \approx 1$ nm (Table 1)). As $\delta_1$ tend to $0$, we obtain electro-neutrality in the spine with constant concentration $c^+(r,t) \approx c^-(r,t) \approx c_{head}(t)$, and constant potential $\Phi(r,t) \approx \Phi_{head}(t)$ (Fig. 1a).

This constant potential approximation in the bulk was also confirmed in recent numerical simulations using finite element, steady-state simulations (11), and is true for the entire spine microdomain, barring a thin boundary layer near the membrane- i.e. the Debye layer (Fig. 1a, inset). To obtain the full solution for the potential and the ion concentrations inside the entire spine head domain (i.e. bulk and boundary layer), we compute the inner solutions near the membrane that both match the boundary conditions and the asymptotic solutions in the bulk. We find that, due to the small electrical permittivity of the membrane, the maximal potential drop occurs across the membrane bilayer. The computed bulk potential is then given by (see SI-I-B for details),

$$\Phi_{head}(t) = \frac{n^+(t) - n^-(t)}{4\pi c_m R^2} \quad (4)$$

Here $n^+(t)$ and $n^-(t)$ are the total number of positive and negative ions inside the spine head at time $t$, and $c_m$ is the membrane capacitance per unit of surface. Typically, $c_m \approx 0.01\ \mathrm{Fm}^{-2}$ (Table 1), and therefore small differences between the total number of positive and negative charges inside the head lead to significant changes of the spine head potential. For example, inside a spherical spine head with radius R = 500 nm, the resting potential $\Phi_0 \approx -60$ mV corresponds to a net excess of $\approx 12{,}000$ negative charges, while the total number of

ions is equal to $\frac{4}{3}\pi R^3 c_0 \approx 50x10^6$ ions. We thus conclude that, due to the small capacitance of the spine head, the entry of few positive charges during synaptic input will result in a rapid depolarization.

The kinetics of ion concentration and potential inside the spine head critically depends on the ionic fluxes with the parent dendrite across the neck. To analyze these fluxes, we followed the methodology developed for modeling ion channels (37, 38) and reduced PNP equations to one-dimensional equations along the neck's principal axis from the spine head (l = 0) to the dendritic shaft (l = L) (Fig. 1a, see SI-II-A for details). For positive and negative ions, the overall flux $J(l,t,v)$, with $v = \pm 1$ (the valency) comprises of a diffusion $J_{diff}(l,t)$ and current $I(l,t)$ (the drift component)

$$J(l,t,v) = J_{diff}(l,t) - \frac{v}{2} I(l,t) \quad (5)$$

Under electroneutral conditions, the diffusion flux drives an equal amount of positive and negative charges in the same direction, and thus results in no net electrical current. Singular perturbation analysis of PNP equations inside the neck, with $\delta_2 = 2\left(\frac{\lambda_D}{L}\right)^2 \ll 1$, leads to (see SI-II-B for details)

$$J_{diff}(l,t) \approx J_{diff}(t) = \frac{D(c_{head}(t) - c_0)}{\int_0^L S^{-1}(l)dl} \quad (6)$$

and,

$$I(l,t) \approx I(t) = R^{-1}\left(l, c_{head}(t)\right) \frac{\partial \Phi(l,t)}{\partial l} \quad (7)$$

where,

$$R\left(l, c_{head}(t)\right) = \frac{\left(2\gamma D S(l)\right)^{-1} \int_0^L S^{-1}(y)dy}{c_0 \int_0^l S^{-1}(y)dy + c_{head}(t) \int_l^L S^{-1}(y)dy} \quad (8)$$

is the electrical resistance of the neck per unit of length. The total neck resistance is then obtained by integrating the unitary neck resistance $R(l, c_{head}(t))$ from l = 0 to l = L. Here, we highlight the following findings: First, the asymptotic diffusion flux (Eq. 6) is the expression normally used to interpret FRAP experiments. This formulation captures only diffusion and neglects the contribution of the electric field on ion dynamics. Second, the neck resistance is not solely dependent on geometry as assumed in cable theory analysis (Fig. 1c) and described in Eq. 9, which depicts the neck resistance assuming constant ion concentration,

$$R_{neck}(c_0) = \int_0^L R(l, c_0)dl = \frac{\int_0^L S^{-1}(l)dl}{2\gamma D c_0} \quad (9).$$

but also critically depends on the ion concentration inside the spine head (Fig. 1d-e, Eq. 8 & 10).

$$\Phi_{head}(\infty) = R_{neck}(\infty)I(\infty) = \gamma^{-1}\log\left(1 + \frac{LI(\infty)}{2DSc_0}\right) \quad (10)$$

Equation 10 (obtained for constant cross-section$S(l) = S$, See SI-III-B for details) shows that the I-V relationship across the spine neck (Fig. 1d) is highly non-linear, similar to current rectification observed in nanofluidic diodes(39) (Fig. 1d, inset). Here $\infty$ denotes the steady state value for$t \gg \tau_c$. Such a non-linear relationship - a consequence of the PNP, was also observed with finite element simulations (11) of spine neck electrostatics, albeit with the assumption that only positive ions contribute to the overall current. This is an important effect which is in contrast to cable theory where the ion concentration is fixed to $c_0$.

**Fast electrical and slow diffusion dynamics inside the dendritic spine**

During synaptic input, both AMPA and NMDA receptors are activated. For the sake of computational simplicity, we make two assumptions – first, we chose to neglect NMDA receptors given that AMPA receptors are known to be the major source of $Na^+$ current. A second assumption was made with respect to the junction diffusion potentials. It is well known that AMPA receptors are almost equally permeable to sodium and potassium, which do have different mobilities and this difference in mobilities can give rise to a diffusion potential – a form of junction potential. We neglected this contribution and account only for the electrical driving force $-g^+(t)\Phi_{Head}(t)$. Here $g^+(t)$ is the time-dependent conductance of AMPA channels. The ionic influx was thus maximum at resting potential $\Phi_0 \approx -60$ mV and collapsed when the spine head potential increased.

Thus using Eq. 6-8 together with the electrical driving force, we obtained the coarse-grained system of differential equations (see SI-III-A for details)

$$2v_{head}\frac{d\,c_{head}(t)}{dt} = -g^+(t)\Phi_{head}(t) - \frac{2D(c_{head}(t) - c_0)}{\int_0^L S^{-1}(l)dl} \quad (11)$$

and $$c_m s_{head}\frac{d\Phi_{head}(t)}{dt} = -g^+(t)\Phi_{head}(t) + \frac{\Phi_0 - \Phi_{head}(t)}{R_{neck}(c_{head}(t)) + R_{dendrite}} \quad (12)$$

Which we solved self-consistently. Here $v_{head} = \frac{4}{3}\pi R^3$and $s_{head} = 4\pi R^2$ are the volume and the surface area of the spine head respectively, and $R_{dendrite}$ is the dendritic input resistance. Equation (11) describes the gradual increase of ion concentration inside the spine head during channel opening, while equation (12) captures the potential dynamics. Equations

(11) and (12) are non-trivially coupled because (i) ion entry kinetics depends on spine head potential and electrical driving force, and (ii) neck resistance depends on ion concentration. Last, at equilibrium, the steady-state current through the neck is given by, $I(\infty) = g^{+}\Phi_{head}(\infty)$. This relation, together with the equation (12), leads to an implicit equation for the steady state current that is solved numerically (see SI-III-B for details).

The coarse-grained system of equations (11-12) is a slow-fast dynamical system. The time constant of concentration changes $\tau_c = v_{head}\int_0^L S^{-1}(u)du/D \approx 10 - 100$ ms is much longer than the time scale of voltage transients, which is due to the charging/discharging of the spine head (capacitor) through the neck resistance (time constant $\tau_\Phi = c_m s_{head}\left(R_{neck} + R_{dendrite} + \frac{1}{g^{+}(t)}\right) \approx 10 - 100$ µs) (Fig. 1f). Thus, for a Heaviside step input (constant channel conductance) ($g^{+}(t) = g^{+}$), voltage increase is rapid at the onset of ion-channel opening, with significant depolarization values and reaches a plateau given by $\Phi_{head} = \frac{\Phi_0}{1+g^{+}(R_{neck}(c_0)+R_{dendrite})}$ in less than 100 µs (Fig. 2a). We termed the first few hundred microseconds of the transient as the *electrostatic* phase and the millisecond time scale the *diffusion* phase. Concentration changes during the electrostatic phase are negligible, but become significant during the diffusion phase (Fig. 2b). The rapid voltage depolarization during the electrostatic phase causes an increase in neck current which plateaus as voltage reaches a steady state, then subsequently increases with concentration (Fig. 2c). The increase in ion concentration and current as a function of sustained input thus significantly influences the neck electrical resistance (Fig. 2d) resulting in its net reduction. We thereby stress that steady state voltage and net ion concentration depend solely on spine neck geometry, whereas their kinetics is controlled by the size of the spine head, volume and membrane capacitance.

**Highlighting the possible role of electrodiffusion with direct electrical recordings**

Recently, we demonstrated the first direct and spontaneous EPSP measurements from spines using nanopipettes (7). These recordings revealed voltage changes on a millisecond time scale with a fast rising phase (≈ 1 ms), followed by a slower decay phase (≈ 10 ms). A recent study measuring synaptic input currents revealed a similar time scale (14), which clearly indicates that the spine electrical transient is large and fast. These time-scales are much slower than the charging and discharging time constants of the spine head capacitor (tens of micro-seconds). Thus, it is most likely that the rising and decay phases correspond to the opening and closing kinetics of ion channels. We used the time course of this published

data along with models of the rising and decay phase of ion channels (21) to explore the effect of electrodiffusion under different spine geometries. Although these recordings were made on spines with thin long necks, the large, fast, and spontaneous millisecond apart EPSPs could be used as a test input to explore the role of electrodiffusion on different spines geometries. We modeled the rising phase of synaptic conductance $g^{+}(t)$ with a sigmoidal function followed by a mono-exponential decay phase: $g^{+}(t) = \frac{g_0 \exp\left(-\frac{t}{\tau_2}\right)}{1+\exp\left(-\frac{t-\mu}{\tau_1}\right)}$ (Fig. 3a). Fitting the spontaneous electrical activity measured previously in the spine head, we found a rapid opening kinetics (median $\mu = 0.36$ ms and $\tau_1 = 0.1$ ms) followed by a slower decay (median $\tau_2 = 5.5$ ms) (Fig. 3a and Table 1). Given the estimated channel kinetics, we used the coarse grained electro-physiological model (equations (11-12)) to predict the kinetics of the current and ion concentration under different spine geometries (Fig. 3b). We found that the current amplitude correlated with the neck resistance (width), but not with the size of the spine head (Fig. 3c). We also observed that the spontaneous variations of ion concentration and neck resistance were significant (Fig. 3d), particularly within spines with small head (reduced volume) and large necks (high current). The kinetics of concentration variations was much slower than the EPSP time course, and for large EPSPs, we observed that the head concentration did not return to its resting state $c_0$ before the arrival of a second EPSP. We thus predicted that the concentration increase (i.e. resistance decrease) could result in a significant reduction in neck resistance during repeated synaptic stimulations (Supplementary Fig. 1). This finding has one important implication in that, real time electrical resistance is fundamentally different from the passive resistance of the spine neck.

## DISCUSSION

The spine neck is an important barrier to ion diffusion during synaptic transmission, but its role in electrically shaping EPSPs has remained controversial due to the lack and difficulty in performing precise experiments from dendritic spines. This has led to an incomplete and often contradictory understanding of spine electrical properties (6, 7, 9, 10, 13, 16, 40). One way to overcome this handicap is with accurate biophysical models. This is normally achieved with cable theory modeling, which is widely used in simulations of neuronal physiology. However, cable equations neglect the role of electrodiffusion (i.e. electric field effect on ion gradients), which can become appreciable in small neuronal compartments such as spines. Here, we use an electrodiffusion framework and model the electrostatics inside the spine during synaptic stimulation. Following previous efforts using

non electroneutral conditions (33) or numerical simulations (11), here, using singular perturbation theory of the PNP equations to model kinetics, we derive a coarse-grained model that fully captures the coupled dynamics of ion concentration and potential inside the spine head. Specifically, we find that (i) diffusion and electrodiffusion together govern the kinetics of spine excitatory post-synaptic potentials (EPSPs); (ii) the spine geometry plays a key role in shaping the EPSP time course; and, (iii) that the current-voltage relationship across the spine-neck is non-linear, which results in the neck resistance varying as a function of ion concentration. We briefly discuss the functional implications of the above findings.

**Functional implications of electrodiffusion in dendritic spines**

Using a coupled slow-fast dynamical system analysis with a Heaviside step input waveform, we showed that the voltage transient can be divided into an *electrostatic phase* - lasting a few hundred microseconds; and a *diffusion* phase - lasting several milliseconds. This result shows that the electrical voltage rises very fast due to fast charging of the spine head (due to a low membrane capacitance), with a steady-state value determined by $I_{syn} \times R_{neck}$, while the diffusion of ions begins to occur only a few milliseconds later. If the spine EPSP is sufficiently high, it adds a significant electromotive force on the ions driving them out of the neck, contributing to a fast and large synaptic current. We have neglected the effect of junction potentials in this study, which arise as a function of local concentration gradients and mobility differences. Such potentials even if a few millivolts in difference could add or subtract from the EPSP in the spine, thereby changing the net difference in voltage between the head and the dendrite and thus the driving force for current flow. One could speculate that this effect could have fundamental implications in synaptic transmission by changing activation/inactivation curve of ion channels located near the neck-head or neck-dendrite junction via differing potentials along the interface. In addition, such voltage gradients across the spine neck could be further exaggerated by geometrical effects such as local membrane curvature and neck diameter which can either increase or decrease the resistance and diffusional properties.

**Regulation of spine neck resistance by ionic concentration**

The rapid voltage increase during the opening of AMPA receptors drives electrical current through the spine neck. Neck current here corresponds to an exchange between positive ions flowing from the spine head to the dendrite and negative ions flowing from the

dendrite to the spine head. However, a fraction of entering sodium ions remains inside the spine, and their slow diffusion through the neck enables a gradual accumulation inside the head nanodomain during receptors opening. Our model predicts that the currents associated with recorded EPSPs are sufficient to change ion concentration inside the spine by up to 30%. This agrees with recent experiments using fluorescent sodium indicators that reported up to 10 mM concentration increase following the AMPA receptors opening during EPSPs (24) and large synaptic conductance's ranging between 2-8nS measured from spines (14). It is important to point out that we neglected the effect of potassium ions and calcium entering the spine neck, which could further change the electrostatic landscape. For example, potassium ions could enter the spine neck from the dendrite in the event of SK channel dependent shunting (41). This current could counter the decrease in spine neck resistance due to the increased sodium concentration and thus tune the net synaptic current. But, regardless of the effects of other ions, the sodium concentration build-up then leads to a reduced electrical resistance through the neck. Moreover, as diffusive extrusion of accumulated ions from the spine head is relatively slow (ten's to hundreds of milliseconds), we predict that high-frequency synaptic input will lead to a pronounced decrease in neck resistance, as the rate of ion concentration buildup in the spine nanodomain will exceed the rate of diffusion through the neck. Our analysis thus reveals a simple, yet new, physiological mechanism of post-synaptic facilitation at millisecond time scale.

To finish, we speculate that part of the reason that spine neck resistance measurements have been at odds with each other could be due to the enhanced ion concentration in the spine which dynamically changes the resistance. Therefore, in addition to the voltage dynamics in the spine head, the net current through the neck would be influenced by the net ion concentration inside the spine nanodomain.

**Supplementary information (SI) accompanies this manuscript.** SI includes detailed mathematical derivations of the equations presented here in this manuscript

**Acknowledgements:** This work was supported by the NIMH (R01MH101218, R01MH100561). This material is also based upon work supported by, or in part by, the U. S. Army Research Laboratory and the U. S. Army Research Office under contract number W911NF-12-1-0594 (MURI). T.L. was supported by the Fondation pour la Recherche

Médicale and the Philippe foundation. K.J was supported by the Kavli Institute of Brain Science at Columbia.

**Competing Financial Interest**: Authors declare no competing financial interests pertaining to this study.

**Author Contributions**: T.L performed the modeling and analysis. K.J assisted with model development and analysis. R.Y assembled and directed the team, provided guidance, funding, and edited the manuscript. T.L and K.J wrote the manuscript.

**Table 1 : Parameters of the electrodiffusion model**

| Variable | Name | Value | Reference |
|---|---|---|---|
| $e$ | Elementary charge | $\approx 1.6\ 10^{-19}\mathrm{C}$ | |
| $\epsilon_c$ | Cytoplasmic permittivity | 80 (= water) | |
| $\epsilon_m$ | Membrane permittivity | 2 (= phospholipid bilayer) | |
| $\gamma = \frac{e}{k_B T}$ | NP constant | $\approx 37\ \mathrm{V}^{-1}$ | |
| $R$ | Radius of the spine head | $50 - 500$ nm | [12] |
| $L$ | Length of the spine neck | $0.1 - 2$ µm | [12] |
| $a$ | Neck radius | $30 - 100$ nm | [12] |
| $S = \pi a^2$ | Cross section of the spine neck | $0.28 - 3.1\ 10^{-2}\mu\mathrm{m}^2$ | |
| $D$ | Diffusion constant of ions | $0.5\ 10^{-9}\mathrm{m}^2\mathrm{s}^{-1}$ | [19-20] |
| $g_0$ | Maximum synaptic conductance | $1.0 - 8.7$ nS | Fitted to data |
| $c_m$ | Membrane capacitance per unit of surface | $0.01\ \mathrm{Fm}^{-2}$ | [31] |
| $c_0$ | Bulk ion concentration | 150 mM | [31] |
| $\Phi_0$ | Resting membrane potential | $-60$ mV | Fitted to data |
| $\mu$ | Kinetics parameter (1) of ion channel opening (sigmoidal function) | $0.27 - 0.71$ ms | Fitted to data |
| $\tau_1$ | Kinetics parameter (2) of ion channel opening (sigmoidal function) | $0.05 - 0.18$ ms | Fitted to data |
| $\tau_2$ | Kinetics parameter of ion channel closure (mono-exponential) | $3.6 - 5.4$ ms | Fitted to data |

| | | | |
|---|---|---|---|
| $\lambda_D = \sqrt{\frac{\epsilon_c}{2e\gamma c_0}}$ | Debye length | $\approx 1$ nm | |
| $\delta_1 = \left(\frac{\lambda_D}{R}\right)^2$ | Singular perturbation parameter in the spine head | $= 0.02 - 0.002$ | |
| $\delta_2 = \left(\frac{\lambda_D}{L}\right)^2$ | Singular perturbation parameter in the spine neck | $= 0.01 - 0.001$ | |

## Figure Legends

**Figure 1**: ***Electro-diffusion model of dendritic spines*** ***a)*** *Spine geometry. Spine head contains synaptic post-synaptic density and ion channels. Membrane is modeled as an impermeable dielectric with small electrical permittivity compared to cytoplasm ($\epsilon_m \ll \epsilon_c$). At resting state, the spine head is depolarized with negative electrical potential $\Phi_0 \approx -60$ mV. Ion concentration $c_{head}(t)$ varies compared to bulk concentration $c_0$. Thin cylindrical neck links the spine head to the parent dendrite. Equivalent circuit describing the dendritic spine electrostatics is represented. Here $C_m$ denotes the capacitance of the head membrane, $C_{neck}$ and $R_{neck}$ denote the membrane capacitance and the longitudinal cytoplasmic resistance of the spine neck. $C_{dend}$ and $R_{dend}$ denote the membrane and resistance of the dendrite. An additional membrane resistance $R_{leak}$ models the ion leaks through the dendrite membrane. All of which combine to determine the voltage kinetics inside the spine head.* ***b)*** *Ultra-structural images of dendritic spine morphology (data reproduced from [12]).* ***c)*** *Geometrical determinants of passive spine neck resistance.* ***d)*** *I-V curve of dendritic spine for two different neck diameter (140 nm (grey) and 80 nm (black)). The discrepancy between the spine I-V curve (dashed line) and Ohm's law with constant resistance (solid line) is highlighted. For thin and highly resistive neck, the spine behaves like a diode (inset scheme).* ***e)*** *Physiological determinants of spine neck resistance.* ***f)*** *Charge kinetics of spine head capacitor as function of dendritic spine geometry (head and neck radius) and ion concentration.*

**Figure 2.** ***Ionic and voltage dynamics.*** *Slow-fast kinetics of ion concentration and electrical potential within the spine head during a step entry of positive ions (constant synaptic conductance $g^+(t) = Constant = 3\ nS$).* ***a)*** *Log plot of the voltage kinetics within different spine geometries, with large (R = 600 nm, dashed line) and small (R= 300 nm, solid lines) head, and different neck diameters (140 nm (red) and 80 nm (grey)). The electrostatics forces dominate at small time scales ($< 100\ \mu s$) and diffusion at larger time scales (> 1 ms). Note the deflection of the electrical potential due to concentration changes and diffusion.* ***b)*** *Log plot of the concentration kinetics.* ***c)*** *Log plot of the neck current kinetics.* ***d)*** *Log plot of the neck resistance kinetics. Notice the drop in neck resistance as ion concentration increases.*

**Figure 3.** ***Experimental match of model***. ***a-*** *Kinetics of channel opening (sigmoidal function, parameters $\mu$ and $\tau_1$) and closure (mono-exponential function, parameter $\tau_2$) are fitted to spontaneous voltage recordings inside dendritic spines using nanopipettes[9]. The voltage profile is fit with the electrodiffusion model presented in this paper* ***b)*** *Schematics of the different spine geometries considered to see the effect of the experimental EPSP magnitude and time course.* ***c)*** *Current estimation as a function of spine geometry using estimated channel kinetics.* ***d)*** *Dynamics of concentration and neck resistance as reflected by coarse-grained electro-diffusion model during spontaneous spine activity. Notice that spines with small head and large necks will see the maximal effect of concentration change on neck resistance.*

1. Harris, K. M., and S. Kater. 1994. Dendritic spines: cellular specializations imparting both stability and flexibility to synaptic function. Annual review of neuroscience 17:341-371.
2. Yuste, R. 2011. Dendritic Spines and Distributed Circuits. Neuron 71:772-781.
3. Yuste, R., and T. Bonhoeffer. 2001. Morphological changes in dendritic spines associated with long-term synaptic plasticity. Annual review of neuroscience 24:1071-1089.
4. Yang, G., F. Pan, and W.-B. Gan. 2009. Stably maintained dendritic spines are associated with lifelong memories. Nature 462:920-924.
5. Stuart, G. J., and N. Spruston. 2015. Dendritic integration: 60 years of progress. Nature neuroscience 18:1713-1721.
6. Popovic, M. A., N. Carnevale, B. Rozsa, and D. Zecevic. 2015. Electrical behaviour of dendritic spines as revealed by voltage imaging. Nature communications 6.
7. Jayant, K., J. J. Hirtz, I. Jen-La Plante, D. M. Tsai, W. D. De Boer, A. Semonche, D. S. Peterka, J. S. Owen, O. Sahin, and K. L. Shepard. 2017. Targeted intracellular voltage recordings from dendritic spines using quantum-dot-coated nanopipettes. Nature nanotechnology 12:335-342.
8. Grunditz, Å., N. Holbro, L. Tian, Y. Zuo, and T. G. Oertner. 2008. Spine neck plasticity controls postsynaptic calcium signals through electrical compartmentalization. Journal of Neuroscience 28:13457-13466.
9. Acker, C. D., E. Hoyos, and L. M. Loew. 2016. EPSPs measured in proximal dendritic spines of cortical pyramidal neurons. Eneuro 3:ENEURO. 0050-0015.2016.
10. Harnett, M. T., J. K. Makara, N. Spruston, W. L. Kath, and J. C. Magee. 2012. Synaptic amplification by dendritic spines enhances input cooperativity. Nature 491:599-602.
11. Cartailler, J., T. Kwon, R. Yuste, and D. Holcman. 2017. Deconvolution of voltage sensor time series and electro-diffusion modeling of synaptic input in dendritic spines. Neuron (in press).
12. Svoboda, K., D. W. Tank, and W. Denk. 1996. Direct measurement of coupling between dendritic spines and shafts. Science 272:716.
13. Tønnesen, J., G. Katona, B. Rózsa, and U. V. Nägerl. 2014. Spine neck plasticity regulates compartmentalization of synapses. Nature neuroscience 17:678-685.
14. Beaulieu-Laroche, L., and M. T. Harnett. 2017. Dendritic Spines Prevent Synaptic Voltage Clamp. Neuron.
15. Araya, R., J. Jiang, K. B. Eisenthal, and R. Yuste. 2006. The spine neck filters membrane potentials. Proceedings of the National Academy of Sciences 103:17961-17966.
16. Kwon, T., M. Sakamoto, D. S. Peterka, and R. Yuste. 2017. Attenuation of Synaptic Potentials in Dendritic Spines. Cell Reports 20:1100-1110.
17. Arellano, J. I., R. Benavides-Piccione, J. DeFelipe, and R. Yuste. 2007. Ultrastructure of dendritic spines: correlation between synaptic and spine morphologies. Frontiers in neuroscience 1:131.
18. Segev, I., and W. Rall. 1998. Excitable dendrites and spines: earlier theoretical insights elucidate recent direct observations. Trends in neurosciences 21:453-460.
19. Koch, C. 1984. Cable theory in neurons with active, linearized membranes. Biological cybernetics 50:15-33.
20. Koch, C., and T. Poggio. 1983. A theoretical analysis of electrical properties of spines. Proceedings of the Royal Society of London B: Biological Sciences 218:455-477.

21. Koch, C., and I. Segev. 1998. Methods in neuronal modeling: from ions to networks. MIT press.
22. Jack, J. J. B., D. Noble, and R. W. Tsien. 1975. Electric current flow in excitable cells.
23. Bloodgood, B. L., and B. L. Sabatini. 2005. Neuronal activity regulates diffusion across the neck of dendritic spines. Science 310:866-869.
24. Miyazaki, K., and W. N. Ross. 2017. Sodium dynamics in pyramidal neuron dendritic spines: synaptically evoked entry predominantly through AMPA receptors and removal by diffusion. Journal of Neuroscience 37:9964-9976.
25. Schuss, Z., A. Singer, and D. Holcman. 2007. The narrow escape problem for diffusion in cellular microdomains. Proceedings of the National Academy of Sciences 104:16098-16103.
26. Donahue, B. S., and R. Abercrombie. 1987. Free diffusion coefficient of ionic calcium in cytoplasm. Cell calcium 8:437-448.
27. Kushmerick, M., and R. Podolsky. 1969. Ionic mobility in muscle cells. Science 166:1297-1298.
28. Qian, N., and T. Sejnowski. 1989. An electro-diffusion model for computing membrane potentials and ionic concentrations in branching dendrites, spines and axons. Biological Cybernetics 62:1-15.
29. Savtchenko, L. P., M. M. Poo, and D. A. Rusakov. 2017. Electrodiffusion phenomena in neuroscience: a neglected companion. Nature Reviews Neuroscience 18:598.
30. Sylantyev, S., L. P. Savtchenko, Y. Ermolyuk, P. Michaluk, and D. A. Rusakov. 2013. Spike-driven glutamate electrodiffusion triggers synaptic potentiation via a homer-dependent mGluR-NMDAR link. Neuron 77:528-541.
31. Sylantyev, S., L. P. Savtchenko, Y.-P. Niu, A. I. Ivanov, T. P. Jensen, D. M. Kullmann, M.-Y. Xiao, and D. A. Rusakov. 2008. Electric fields due to synaptic currents sharpen excitatory transmission. Science 319:1845-1849.
32. Schuss, Z., B. Nadler, and R. S. Eisenberg. 2001. Derivation of Poisson and Nernst-Planck equations in a bath and channel from a molecular model. Physical Review E 64:036116.
33. Holcman, D., and R. Yuste. 2015. The new nanophysiology: regulation of ionic flow in neuronal subcompartments. Nature Reviews Neuroscience 16:685-692.
34. Cartailler, J., Z. Schuss, and D. Holcman. 2017. Electrostatics of non-neutral biological microdomains. Scientific Reports 7:11269.
35. Jayant, K., K. Auluck, M. Funke, S. Anwar, J. B. Phelps, P. H. Gordon, S. R. Rajwade, and E. C. Kan. 2013. Programmable ion-sensitive transistor interfaces. II. Biomolecular sensing and manipulation. Physical Review E 88:012802.
36. Jayant, K., K. Auluck, S. Rodriguez, Y. Cao, and E. C. Kan. 2014. Programmable ion-sensitive transistor interfaces. III. Design considerations, signal generation, and sensitivity enhancement. Physical Review E 89:052817.
37. Chen, D., J. Lear, and B. Eisenberg. 1997. Permeation through an open channel: Poisson-Nernst-Planck theory of a synthetic ionic channel. Biophysical Journal 72:97-116.
38. Kosińska, I., I. Goychuk, M. Kostur, G. Schmid, and P. Hänggi. 2008. Rectification in synthetic conical nanopores: A one-dimensional Poisson-Nernst-Planck model. Physical Review E 77:031131.
39. Schoch, R. B., J. Han, and P. Renaud. 2008. Transport phenomena in nanofluidics. Reviews of Modern Physics 80:839-883.

40. Yuste, R. 2013. Electrical compartmentalization in dendritic spines. Annual review of neuroscience 36:429-449.
41. Ngo-Anh, T. J., B. L. Bloodgood, M. Lin, B. L. Sabatini, J. Maylie, and J. P. Adelman. 2005. SK channels and NMDA receptors form a Ca2+-mediated feedback loop in dendritic spines. Nature neuroscience 8:642-649.

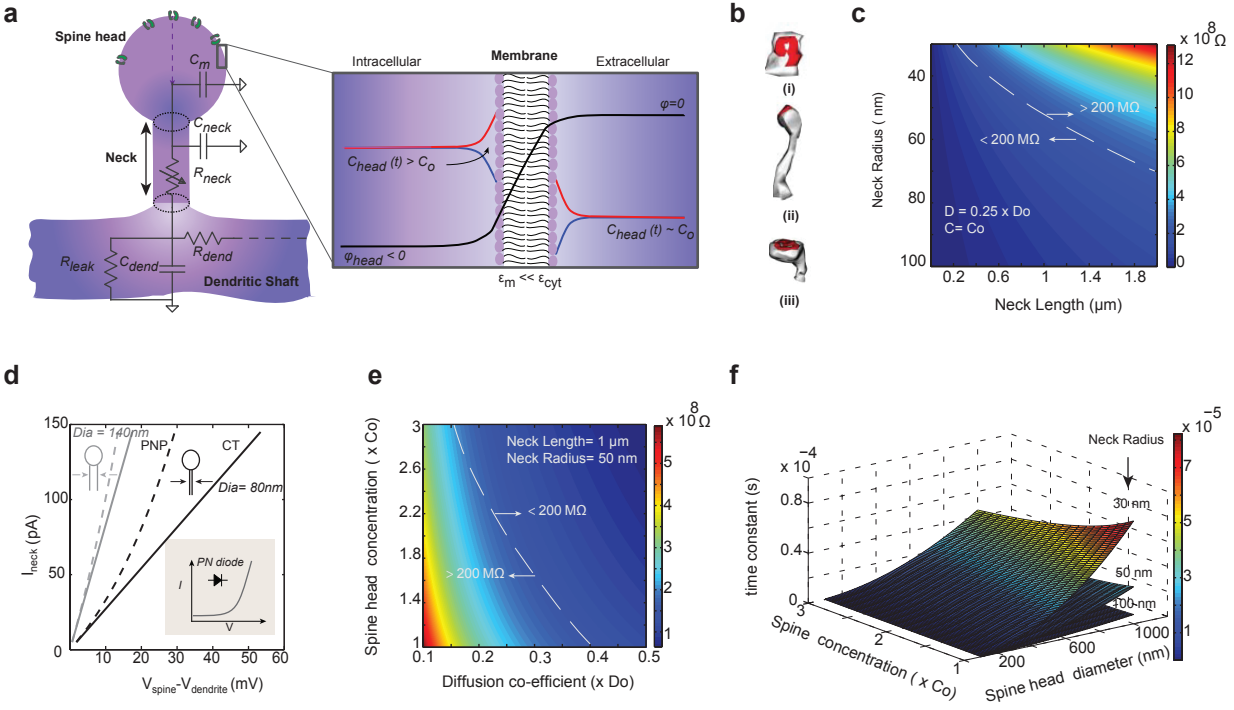
a
Spine head
$C_m$
$C_{neck}$
Neck
$R_{neck}$
$R_{dend}$
$R_{leak}$
$C_{dend}$
Dendritic Shaft
Intracellular
Membrane
Extracellular
$\varphi=0$
$C_{head}$ (t) > $C_o$
$C_{head}$ (t) ~ $C_o$
$\varphi_{head} < 0$
$\varepsilon_m << \varepsilon_{cyt}$
b
(i)
(ii)
(iii)
c
x $10^8$ Ω
Neck Radius ( nm)
Neck Length (μm)
> 200 MΩ
< 200 MΩ
D = 0.25 x Do
C= Co
d
Dia = 140nm
PNP
CT
Dia= 80nm
PN diode
$I_{neck}$ (pA)
$V_{spine}$-$V_{dendrite}$ (mV)
e
x $10^8$ Ω
Neck Length= 1 μm
Neck Radius= 50 nm
< 200 MΩ
> 200 MΩ
Spine head concentration ( x Co)
Diffusion co-efficient (x Do)
f
x $10^{-4}$
x $10^{-5}$
Neck Radius
30 nm
50 nm
100 nm
time constant (s)
Spine concentration ( x Co)
Spine head diameter (nm)

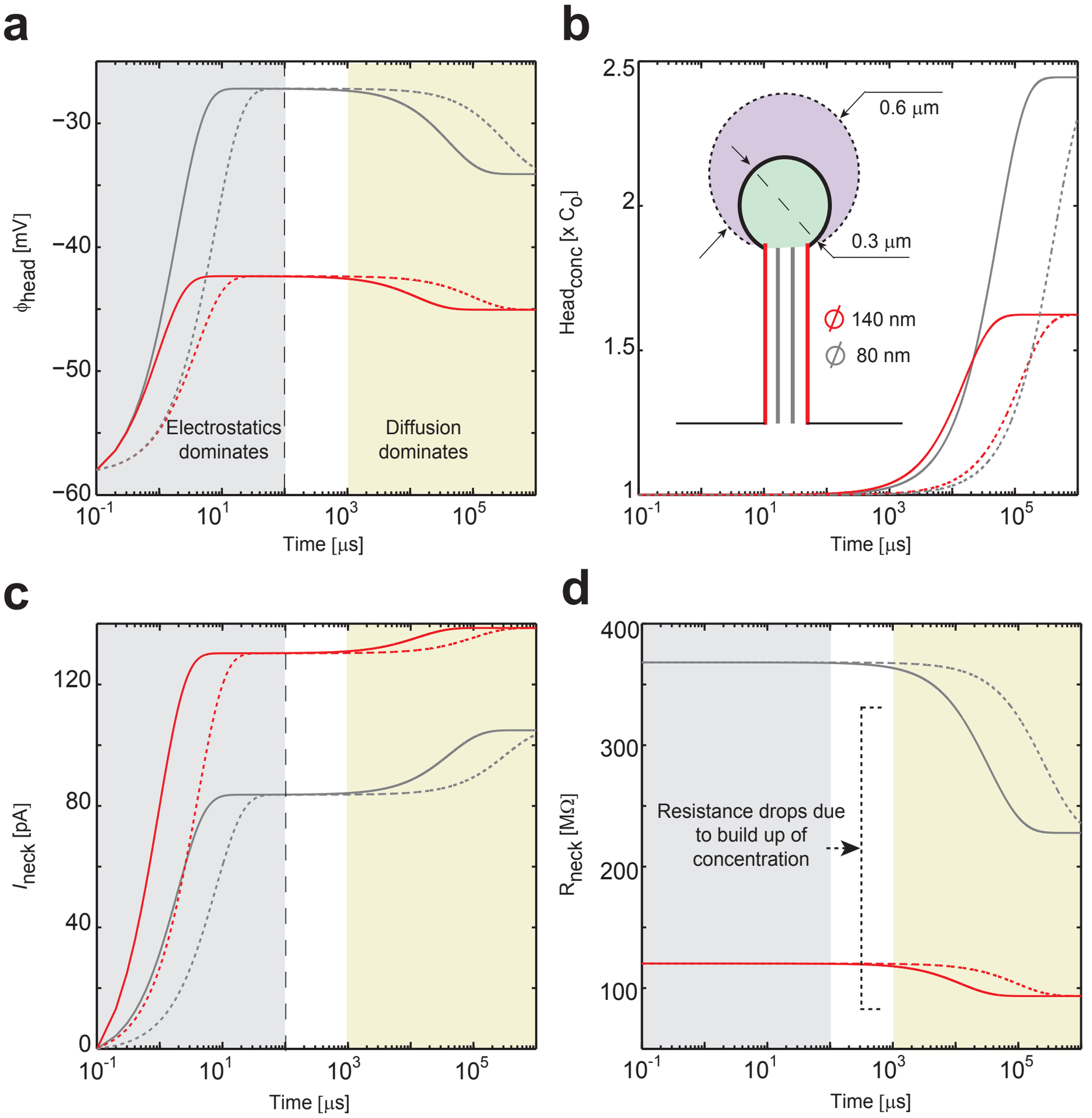
a
b
c
d
$\phi_{head}$ [mV]
−30
−40
−50
−60
Electrostatics dominates
Diffusion dominates
$10^{-1}$
$10^{1}$
$10^{3}$
$10^{5}$
Time [μs]
$Head_{conc}$ [x $C_0$]
2.5
2
1.5
1
0.6 μm
0.3 μm
∅ 140 nm
∅ 80 nm
$I_{neck}$ [pA]
120
80
40
0
$R_{neck}$ [MΩ]
400
300
200
100
Resistance drops due to build up of concentration

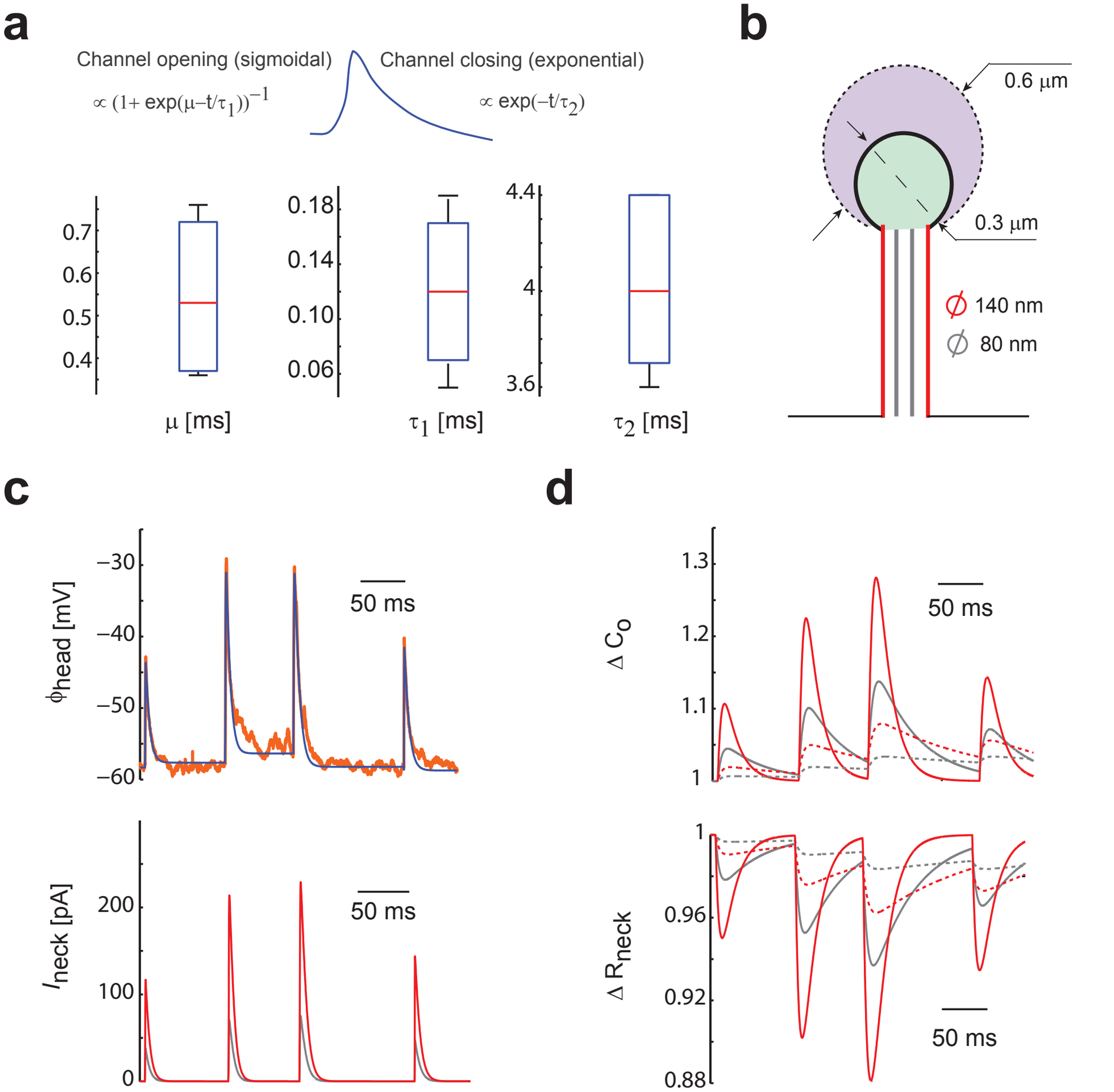
a
Channel opening (sigmoidal)
∝ (1+ exp(μ–t/τ1))−1
Channel closing (exponential)
∝ exp(–t/τ2)
0.7
0.6
0.5
0.4
μ [ms]
0.18
0.14
0.10
0.06
τ1 [ms]
4.4
4
3.6
τ2 [ms]
b
0.6 μm
0.3 μm
∅ 140 nm
∅ 80 nm
c
ϕhead [mV]
−30
−40
−50
−60
50 ms
Ineck [pA]
200
100
0
50 ms
d
Δ Co
1.3
1.2
1.1
1
50 ms
Δ Rneck
1
0.96
0.92
0.88
50 ms